β-Lactoglobulin Fibers under Capillary Flow

Valeria Castelletto* and Ian W. Hamley

School of Chemistry, The University of Reading, P.O. Box 224, Whiteknights, Reading RG6 6AD, United Kingdom

Received June 20, 2006; Revised Manuscript Received August 4, 2006

We describe the capillary flow behavior of gels of β-lactoglobulin (β-lg) containing droplets of fibrils and the shear flow alignment of β-lg fibers in dilute aqueous solutions. Polarized optical microscopy and laser scanning confocal microscopy are used to show that capillary shear flow does not affect the fibril droplet sizes in the β-lg gels, the system behaving in this respect as a solution of compact colloidal particles under shear flow. Small-angle X-ray scattering (SAXS) on dilute aqueous solutions indicates that the fibers can be initially aligned under capillary shear, but this alignment is lost after 18 min of shear. Transmission electron microscopy experiments on the samples studied by SAXS suggest that the loss of orientation is due to a shear-induced breakup of the swollen fibril network. Dynamic and static light scattering on dilute β-lg fibril aqueous solutions are used to show that before shear β-lg fibrils behave as strongly interacting semiflexible polymers, while they behave as weakly interacting rods after 18 min of capillary shear.

Introduction

The ability of certain proteins to form amyloid fibrils has been the focus of intensive research. The formation of amyloid fibers can occur in human tissues affected by several neurological amyloid diseases,[1,2] but amyloid fibers can also have physiological functions, for example, in blood clotting.[3] Amyloid fibrils are also present in food protein gels obtained under certain heating, pH, and ionic strength conditions.[4−15] Understanding gel structure and gelation is of major importance in several food processing applications.

Bovine β-lactoglobulin (β-lg) is a globular protein, which is important in the food industry because of its high content in whey.[16] This protein forms fine-stranded, transparent gels under heating, at pH 2, and at low ionic strength. At pH 2, β-lg presents a purely positive surface charge. The monomers interact through repulsive electrostatic interactions, apparently leading to the formation of transparent gels with a relatively open network structure of amyloid fibers.[8]

Although the formation of the gels mentioned above has been extensively studied in the literature,[8,15,17] we are only aware of only one prior study on the influence of shear flow on fibril self-assembly.[18] The shear flow behavior of β-lg fibril gels and solutions at pH 2 was studied using fluorescence spectroscopy and atomic force microscopy (AFM).[18] It was shown that preformed β-lg fibers break down at high shear rates.

The purpose of the present article is to describe studies on the flow alignment of preformed β-lg fibers under capillary flow. The samples were studied using polarized optical microscopy (POM), laser scanning confocal microscopy (LSCM), small-angle X-ray scattering (SAXS), dynamic (DLS) and static (SLS) light scattering, and transmission electron microscopy (TEM).

The protocol to produce preformed β-lg fibers studied in this work is similar to that already used in prior flow experiments.[18] However in the previous work the samples were sheared using a Couette (concentric cylinder) geometry while in this work we investigate capillary flow. In addition, in our work in situ SAXS experiments provide information about the shear flow alignment of the sample, while POM and LSCM give information on order at a length scale larger than that previously used AFM. Light scattering and TEM experiments provide information on the fibril shape and dimensions of the particles before and after shear.

* Author to whom correspondence should be addressed. Phone: 44-113-343-6430. Fax: 44-113-343-6551. E-mail: V.Castelletto@reading.ac.uk.

Experimental Section

Materials. β-Lactoglobulin was purchased from Sigma, U. K., and used as received. Rhodamine B, used for LSCM, was bought from Fluka, U. K.

Approximately 2.2 wt % β-lg samples, pH 2, were prepared by mixing controlled amounts of protein and double-distilled deionized water. The pH was fixed by adding an amount of 1 M HCl solution corresponding to an ionic strength of $I = 112$ mM. These samples were placed in sealed tubes and heated in a water bath at 80 °C for 24 h. In this way, a weak, transparent gel was obtained, which was studied by POM and LSCM.

Some of the 2.2 wt % β-lg gels described in the paragraph above were diluted to 0.67 wt % β-lg by adding double-distilled deionized water. These samples correspond to $I = 40$ mM. Diluted samples were studied by SAXS, DLS, and SLS.

All of the samples were studied within 24 h after preparation. In the following, to simplify the presentation of our work, sample A will refer to a 2.2 wt % β-lg sample (pH 2, $I = 112$ mM) heated at 80 °C for 24 h, while sample B will correspond to sample A diluted to 0.67 wt % β-lg ($I = 40$ mM).

Shear Flow Cell. We constructed a capillary flow device, similar to that developed by Bernal and Fankuchen,[19] for use in time-resolved scattering studies of flow-induced alignment. Details of this machine have been given elsewhere.[20] Briefly, the central part of the capillary flow device is a computer-controlled peristaltic pump that allows controlled volume and time dispensing. The flow rate is recorded, and the unit is interfaced to a PC for acquisition of flow rate data. We used borosilicate capillaries with an internal radius of $R = 2$ mm. The flow rate was fixed to $Q = 6$ mL min^{-1} for all of the experiments. This corresponds to a Newtonian shear rate at the wall of $\dot{\gamma} = 4Q/\pi R^3 = 127$ s^{-1}.

Small-Angle X-ray Scattering. Experiments were carried out on beamline 16.1 at the Synchrotron Radiation Source (SRS, Daresbury,

10.1021/bm0605917 CCC: $37.00
Published on Web 12/10/2006

U. K.). The samples were mounted in the shear flow cell mentioned above. Samples were also mounted in a sealed 1-mm-thick liquid cell, with an inner spacer ring to hold liquids, sealed between mica windows.

A wavelength λ of 1.41 Å and a detector−sample distance of 1.2 m were used at the SRS together with a two-dimensional (2D) gas-filled area detector (RAPID). The SAXS data were corrected to allow for sample transmission, background scattering, and detector response.

The shear flow device was positioned such that the flow direction **v** was horizontal (x-axis) in the 2D detector plane.

To analyze the data from the 2D detector, the SAXS data from the flow cell were reduced by radial integration in a 30° vertical angular sector ($I_{\perp}(q)$) or in a radial circular mask (isotropically averaged intensity, $I(q)$). Only the radially averaged SAXS data $I(q)$ were necessary to analyze the data from the liquid cell.

The SAXS intensity $I_s(q)$ of a solution corresponding to a system of weakly interacting spherical objects can be approximated at very low scattering angles by the Guinier law[21]

$$\lim_{q\to 0} I_s(q) = I_s(0)\exp\left(-\frac{q^2 R_G^{\,2}}{3}\right) \quad (1)$$

where $I_s(0)$ is the scattering at $q = 0$ and R_G corresponds to the radius of gyration of the scattering particle and can be evaluated from a Guinier plot of $\ln[I_s(q)]$ versus q^2 in the regime $qR_G < 1$. If the scattering particle has a cylindrical geometry, then eq 1 is no longer valid, and the intensity at very small angles is given by

$$I_s(q) = I_s(0)\exp\left(-\frac{q^2 R_{G,c}^{\,2}}{2}\right) \quad (2)$$

where $R_{G,c}$ is the radius of gyration of the cylinder cross section ($R_{G,c} = R_c/2^{1/2}$; R_c is the radius of the cylinder cross section).[21] Its value can be evaluated from a plot of $\ln[qI_s(q)]$ versus q^2 (a modified Guinier plot for a rodlike particle) in the regime $qR_{G,c} < 1$.

Polarized Optical Microscopy. Images were obtained with a Zeiss Axioskop 40 polarized microscope by placing the sample between crossed polarizers. Samples were placed between a glass slide and a coverslip before capturing the images with a Canon G2 digital camera.

Laser Scanning Confocal Microscopy. Experiments were performed on a Leica TCS SP2 confocal system mounted on a Leica DM-IRE2 upright microscope, using a 20× objective with a 0.4NA numerical aperture. For confocal microscopy experiments, β-lg was dyed using rhodamine B dissolved in double-distilled deionized water with a dye/protein ratio of approximately 1:2000. The excitation wavelength generated by an argon laser was 514 nm, while the emission detection was in the range of 558−617 nm. Samples were examined in the flow cell, before and after shear, or they were put between a glass slide and a coverslip.

Dynamic and Static Light Scattering. Experiments were performed using an ALV CGS-3 system with 5003 multidigital correlator. The light source was a 20 mW He−Ne laser, linearly polarized, with λ = 633 nm. Toluene was used to calibrate the Rayleigh ratio as per standard procedures for SLS. Scattering angles in the range $40° \le \theta \le 150°$, with $\Delta\theta = 10°$, were used for all of the experiments. DLS was performed for correlation time scales of 2.5×10^{-4} ms $\le \tau \le 4.0 \times 10^3$ ms. Samples were prepared in standard 0.5 cm diameter cylindrical glass cells. They were filtered through 0.20 μm Anotop filters from Whatman.

DLS experiments measured the intensity correlation function

$$g^{(2)}(q,t) = \langle I(q,0)I(q,t)\rangle_\tau / \langle I(q,0)\rangle_\tau^{\,2} \quad (3)$$

where $q = [4\pi n \sin(\theta/2)]/\lambda$ is the scattering vector (λ is the vacuum wavelength of the radiation and n is the refractive index of the medium) and $I(q,t)$ is the intensity scattered by the sample in the course of an experiment of duration τ.

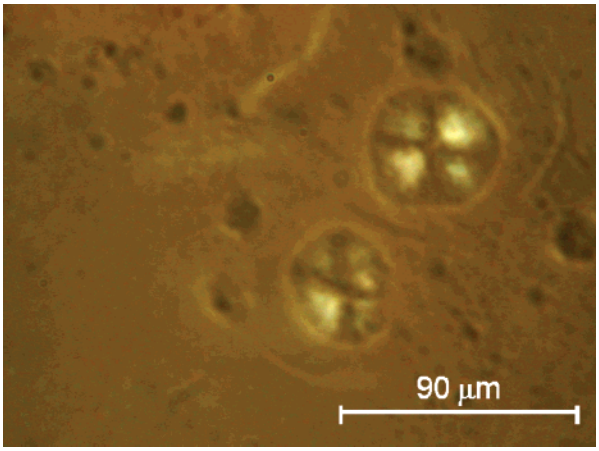

Figure 1. Polarized optical microscopy corresponding to sample A.

The measured intensity correlation function is related to the field correlation function, $g^{(1)}(q,t)$, by the Siegert relationship[22]

$$g^{(2)}(q,t) = 1 + [g^{(1)}(q,t)]^2 \quad (4)$$

The normalized SLS intensity was measured as $I_{SLS} = R/Kc$, where K is the optical contrast factor and c is the concentration of the sample. The term R in I_{SLS} is the Rayleigh ratio, corrected by background subtraction and normalized by the scattering of the toluene.

Transmission Electron Microscopy. Experiments were done using a Philips CM20 transmission electron microscope, operating at 200 and 80 kV for samples A and B, respectively. Samples were stained using 1 wt % methylamine tungstate (Agar Scientific, U. K.), while polyvinyl formal grids (Agar Scientific, U. K.) were used to support the samples. To prepare the samples for TEM observation, one drop of sample was put onto a grid, followed by one drop of staining solution. The grid was left to dry in a fume cupboard for a few minutes after drop deposition.

Results and Discussion

Sample A was studied by POM. The photographs show spherical droplets, with an average diameter of $d_i \approx 57$ μm, dispersed in an isotropic matrix (Figure 1). The particular droplet extinction pattern in Figure 1 indicates a radial configuration of directors within nematic domains that correspond to fibrils aligned in a concentric configuration. Similar structures, with the characteristic cross-shaped extinction pattern shown in Figure 1, have already been observed by POM and TEM for concentrated β-lg solutions containing salt[23] and for amyloid fibrils of bovine insulin.[24] In addition, it has been reported that droplets observed for bovine insulin[24] contain a large quantity of amyloid fibrils and they arise as a consequence of the self-assembly of preformed fibrils into nematic domains.

LSCM revealed, for sample A placed between a glass slide and a coverslip, that the matrix in Figure 1 comprises β-lg fibers (Figure 2a). The width, d, of the fibers in Figure 2a, was measured using ImageJ software, resulting in $d = 4-6.5$ μm. A cluster of fibril droplets can also be observed in the top right-hand corner of Figure 2a. Sample A was placed in the flow cell and sheared for 20 min. The geometry of the capillary did not allow focusing by LSCM on the fibril matrix. Nevertheless, LSCM could be used to observe the spherulites suspended in the fibril matrix for the sample in the flow cell. Figures 2b and 2c show the same droplets shown in Figure 1, before and after the sample was sheared for 20 min. It was possible to observe that the average radius of the droplets was not noticeably affected by the shear.

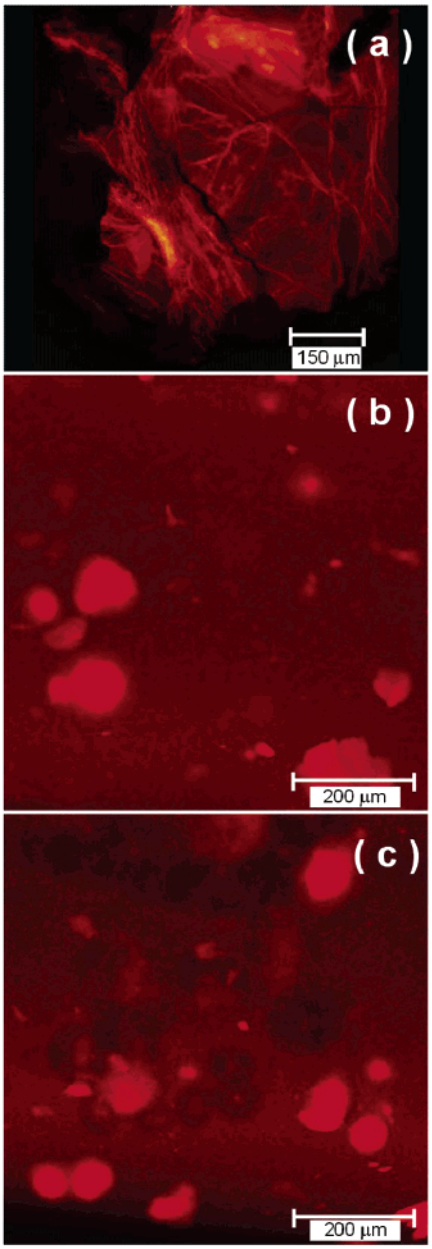

Figure 2. LSCM images of sample A. (a) Fibril matrix observed for a sample between a glass slide and a cover slip. Nematic droplets (b) before and (c) after shear observed for the sample in the capillary flow cell. The flow direction is approximately horizontal.

Although POM and LSCM proved to be useful to study the macroscopic phase separation, they do not provide information on the influence of capillary shear flow on the fibril matrix. Indeed, there are two alternative procedures to study the behavior of the fibril matrix under shear: It is possible to remove the spherulites from sample A by filtration,[25] or alternatively, sample A can be diluted since the number of nematic spherulites and their size decrease with decreasing concentration.[23] We decided to dilute sample A to 0.67 wt % β-lg (sample B), which corresponds to the lower concentration boundary for the two-phase system with nematic droplets immersed in a fibril matrix, measured at $I = 40$ mM and pH 2.[23]

The capillary shear flow behavior of sample B was then studied by SAXS and light scattering. The concentration of sample B is high enough to provide a reasonable SAXS pattern and low enough to prevent any contribution from residual fibril droplets to the SAXS signal. Regarding light scattering experiments, filtration of the samples previous to the experiments should remove fibril droplets from the sample.

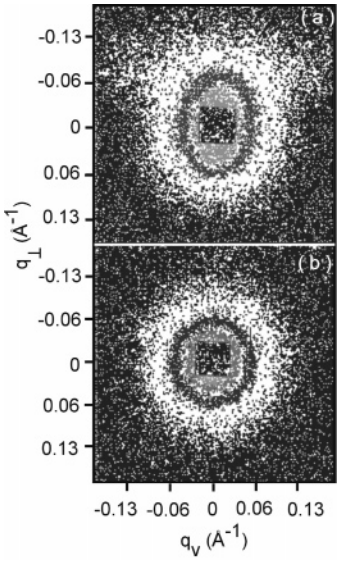

Figure 3. SAXS patterns obtained for sample B (a) 2 and (b) 18 min after the capillary shear flow was initiated.

Simple B was initially mounted in a liquid cell and studied by SAXS. A standard Guinier plot could be constructed (data not shown), from which a radius of gyration $R_G = 17$ Å was calculated, in good agreement with results previously reported in the literature from small-angle neutron scattering studies.[26]

Sample B was then studied in the flow cell. The sample was subjected to capillary flow for 60 min. Figures 3a and 3b show the SAXS data collected for the sample under shear at the beginning of the shear flow and 18 min after the shear flow had started. According to Figure 3, the β-lg fibers initially orient under shear flow, but this orientation is lost after 18 min. The SAXS pattern remained similar to that shown in Figure 3b for the following 42 min under shear flow, showing that the alignment of the fibers under shear flow was not recovered during the course of the experiment. Subsequent observations of the SAXS patterns, spanning 60 min after the shear was stopped, showed that the scattering signal remained isotropic.

To quantify the anisotropy of the SAXS patterns, the isointensity lines derived from the SAXS patterns were roughly approximated, at sufficiently high q, by concentric ellipses or circles. The ratio $\Delta = A/B$ of the long axis A to the short axis B of an elliptical contour line defines the anisotropy of the scattering objects ($A = B$ for circular patterns). In our experiments, the long axis of the ellipses is always parallel to the vertical axis on the detector. Therefore, $\Delta > 1$ corresponds to an anisotropic scattering object elongated in the direction of flow. The anisotropy of the SAXS patterns during shear flow is plotted as a function of time in Figure 4a. In agreement with the paragraph above, Δ decreases from 1.3 to 1.1 during the first 18 min, and it remains stable and equal to 1 during the last 42 min.

The intensities $I_\perp(q)$ and $I(q)$ were also calculated from the 2D SAXS spectra and used to calculate R_c from the modified Guinier plots. Figure 4b shows two representative modified Guinier plots, for the oriented fibers at time $t = 2$ min (anisotropic SAXS pattern, $\Delta > 1$) and the isotropic system at $t = 20$ min (isotropic SAXS pattern, $\Delta = 1$). It should be noted that our results suggest that the isotropic system consists of fibers, since it was possible to obtain a satisfactory modified Guinier plot using $I(q)$ from the isotropic SAXS pattern (Figure 4b).

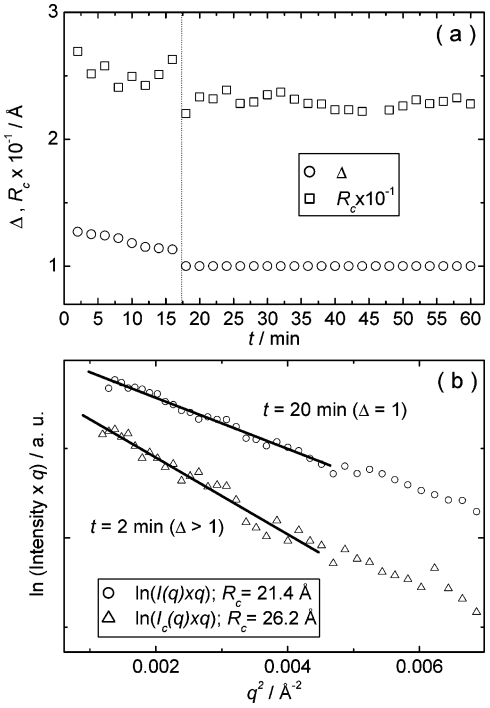

Figure 4. (a) Time dependence of the SAXS pattern anisotropy and radius of the cylinder cross section, for sample B under shear. (b) Modified Guinier plots obtained for sample B at 2 and 20 min after the capillary shear flow was initiated.

The data in Figure 4a shows that R_c for the oriented fibers ($\Delta > 1$) slowly decreases from 27 Å during the first 18 min, while it remains nearly equal to 23 Å for the nonoriented fibers ($\Delta = 1$). The change in R_c upon changing the external shear flow constraint might be indirect evidence for rearrangements of the internal structure of the fibers, or it can arise due to a degree of polydispersity in R_c. In particular, the decrease in the thickness of the fibers before shear from $d = 4.5-6$ μm for sample A to $2R_c = 54$ Å for sample B supports the hypothesis of, at least, concentration-dependent rearrangements of the internal structure of the fibrils.

However, it is not possible to obtain details of the internal structure of the fibers using SAXS. Nevertheless, it is possible to confirm that R_c values in Figure 4a are in good agreement with data in the literature. Previous AFM experiments on β-lg fibers in a film dried from solution A revealed that the fibers had $R_c \approx (20-25)$ Å before and after shearing in Couette flow at 300 s^{-1} for 240 min[18]

Figure 5a shows the TEM image obtained for sample B before shear. As expected, the sample presents a fibril structure, and there are no nematic droplets dispersed in the fibril matrix. The average thickness of the fibrils is 58 Å, in good agreement with the value obtained by SAXS. Sample B was subjected for 20 min to shear flow in the capillary flow cell. The TEM image obtained for the sample after shear is shown in Figure 5b. A qualitative inspection of Figure 5 reveals that the mesh size of the fibril network in Figure 5b is smaller than the mesh size in Figure 5a, pointing to a reduction in the contour length of the fibrils under shear flow. However, Figure 5b shows fibrils with thicknesses up to 70 Å. This thickness is higher than that measured by SAXS after 18 min of shearing time ($2R_c = 46$ Å), because the fibrils are affected by a large polydispersity in R_c, as mentioned above in relation to Figure 4.

It should be mentioned that the apparent fibril dimensions from TEM may be influenced by preparation techniques. For example, they may be affected by drying or staining artifacts.

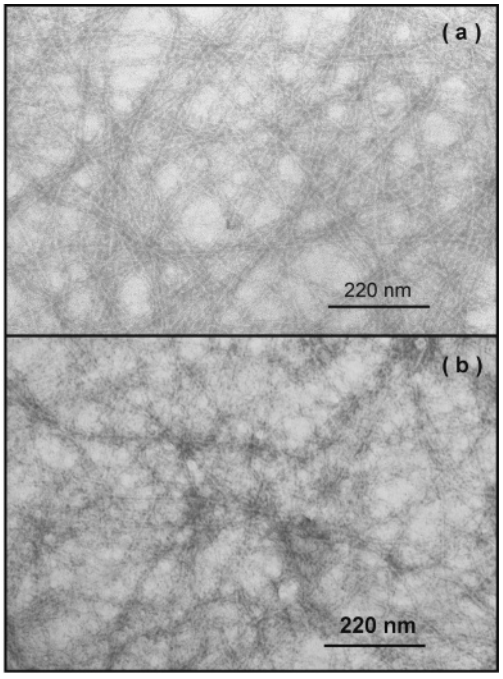

Figure 5. TEM of fibrils obtained for sample B (a) before and (b) after subjecting the sample to capillary shear flow for 20 min.

In an attempt to extract additional information about the sample structure before and after capillary flow, sample B was studied by DLS and SLS. The light scattering setup does not allow for simultaneous shear flow/scattering experiments. Therefore, light scattering experiments were undertaken before and after shearing the sample in the flow cell for 20 min. The formation of β-lg fibers after heat denaturation at 80 °C, pH 2, and different ionic strengths has already been studied by DLS in the literature, on time scales up to 200 min.[8,15] In that work, only one relaxation time was used to describe the dynamics.

On the basis of the information above, our DLS curves should be dominated by only one apparent diffusion time. Therefore we decided to model our DLS curves using only one relaxation time. Using a stretched exponential to model $g^{(1)}(q,t)$ allows for a spectrum of relaxation times resulting from the internal modes of the aggregates

$$g^{(1)}(q,t) = C \exp(-t/\tau_\beta)^\beta \qquad (5)$$

where τ_β is a characteristic decay time of the system, C is a constant, and the exponent β ($0 \le \beta \le 1$) is a measure of the width of the corresponding distribution of relaxation times. The smaller the value of β, the broader the distribution. The mean characteristic time, $\bar{\tau}_\beta$, of the stretched exponential mode is given by $\bar{\tau}_\beta = (\tau_\beta/\beta)\Gamma(1/\beta)$ where $\Gamma(1/\beta)$ is the gamma function. The corresponding decay time is $\bar{\Gamma}_\beta = 1/\bar{\tau}_\beta$.

Figure 6 shows some representative examples for $g^{(1)}(q,t)$ calculated according to eq 4 and fitted using eq 5. The dependence of the parameters extracted from the fits (β and apparent diffusion coefficient $D = \bar{\Gamma}_\beta/q^2$) with q is shown in Figure 7. The apparent diffusion coefficient has previously been measured by DLS on dilute samples of β-lg (incubated at 80 °C for 2.5−11 h), at pH 2 and $I = 13$ mM, providing $D \approx 10^{-12}$ m^2s^{-1},[8] in good agreement with the results in Figure 7a.

Figure 7a shows that within the experimental error the q-dependence of D for the sample under shear can be fitted to $D \propto q^{-0.7}$, which is close to the result expected for semiflexible polymers.[8] Figure 7b shows that the q-dependence of the apparent diffusion coefficient changes to $D \propto q^{-1.4}$ after sample

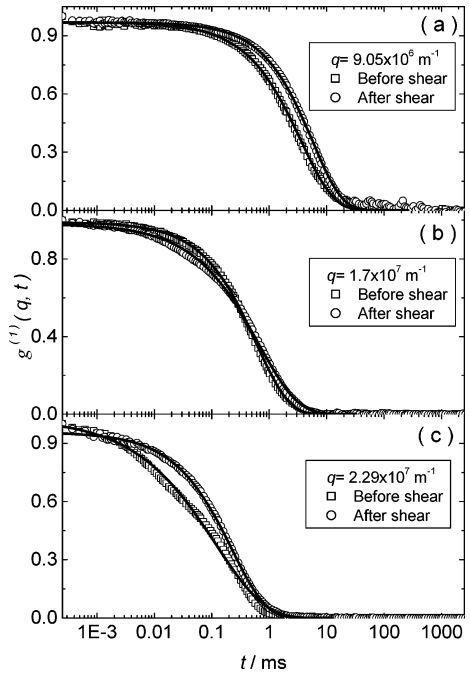

Figure 6. DLS data (□) before and (○) after subjecting the sample to capillary flow for 20 min. The full lines correspond to the fitting according to eq 5, while the scattering angle for each experiment is indicated in the graph.

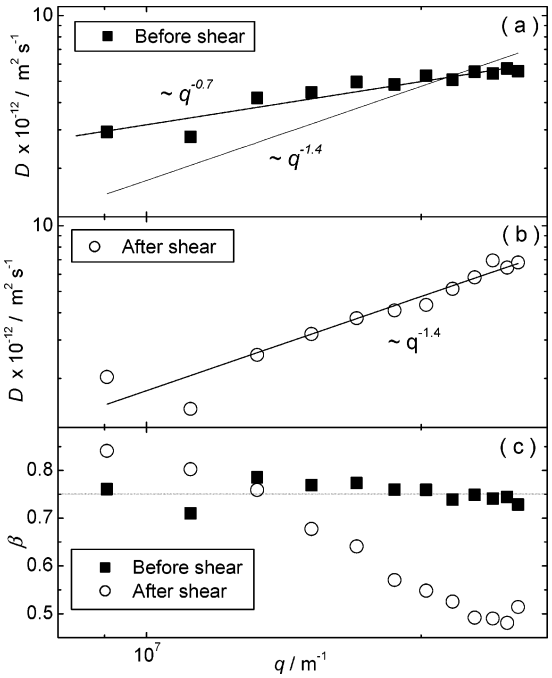

Figure 7. Scattering vector dependence of the apparent diffusion coefficient (a) before and (b) after shearing sample B for 20 min. (c) Stretched exponential exponent β obtained from the fitting of the DLS using eq 5. The full lines in parts a and b correspond to the fitting of the data with a decay power law. The slope $q^{-1.4}$ is shown in part a for comparison. The dotted line in part c corresponds to the averaged value obtained for the sample before shear, which matches the theoretical value of β for semiflexible polymers.[27]

B has been subjected to capillary shear flow for 20 min. This q-dependence is closer than $D \propto q^{-0.7}$ to the result expected for short rigid cylinders ($D \propto q^{-2}$), probably being a consequence of the fibril morphology change due to shear-induced degradation. Regarding the value of β shown in Figure 7c, for sample B before shear, it oscillates around the value expected

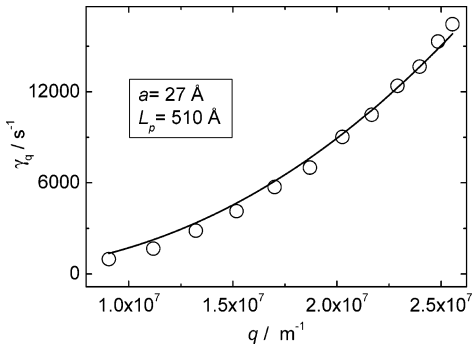

Figure 8. Angular dependence of the γ_q coefficient. The full line corresponds to a fit using eq 7. The value of the parameter extracted from the fitting is indicated.

for a system of semiflexible polymers ($\beta = {}^3/_4$).[27] In contrast, β decreases with increasing q for the sample subjected to shear flow. The coefficient β, at a sufficiently high q, is smaller after shear than it is before shear. A smaller value of β indicates a wider distribution of relaxation times. Then, the decrease of β under shear flow might indicate an increase in polydispersity of the β-lg fibers due to shear-induced breakup.

The DLS data indicated that the β-lg fibers behave as semiflexible polymers for the sample before shear. It is therefore worth applying the Kroy and Frey theory for semiflexible polymers,[27] to calculate the persistence length of the fibers L_p, directly proportional to the fibril bending elastic constant,[28] which could be compared to the shear flow strength to understand the fiber degradation process under shear. According to this theory, at long times the correlation function can be modeled according to

$$g^{(1)}(q,t) = g^{(1)}(q,0)\exp\left(-\frac{\Gamma(1/4)}{3\pi}(\gamma_q t)^{3/4}\right) \qquad (6)$$

with

$$\gamma_q = \frac{k_B T q^{8/3}}{4\pi\eta_s L_p^{1/3}}(5/6 - \ln(qa)) \qquad (7)$$

where $k_B = 1.38 \times 10^{-23}$ J K^{-1} is the Boltzmann constant and η_s is the viscosity of the solvent (water), taken as 8.9×10^{-4} Pa s for $T = 25$ °C.[29] The parameter a in eq 7 corresponds to the hydrodynamic diameter of the fibers.

The values of γ_q were calculated using the characteristic decay times already obtained from the fits of eq 5 to the DLS data, assuming that $(1/\tau_\beta)([\Gamma({}^1/_4)]/3\pi)^{-\beta} = \gamma_q$. The obtained γ_q coefficients are plotted in Figure 8 as a function of q together with a fit to eq 7. To fit eq 7 to the experimental data, the hydrodynamic radius of the fibers was approximated by the value obtained for R_c after 2 min of shearing (Figure 4a). In this way, fixing $a = 2R_c = 54$ Å, the persistence length in eq 7 was the fitting parameter, providing $L_p = 510$ Å for the β-lg fibers before shear.

TEM experiments on β-lg fibrils obtained from 2−8 wt % gels ($I = 10-80$ mM) heated for 10 h at 80 °C showed fibrils with averaged contour lengths of $L_c = 4500$ nm.[23] AFM and TEM on β-lg fibers induced by incubation of a 5 wt % pH 2 solution at 80 °C for 18 h indicated fibers that were 100−2000 nm in length.[17] Much shorter fibers than those reported here were found by AFM experiments on β-lg fibers similar to those in sample B, showing that the averaged contour length of the fibers before shear is $L_c = 450$ nm.[18]

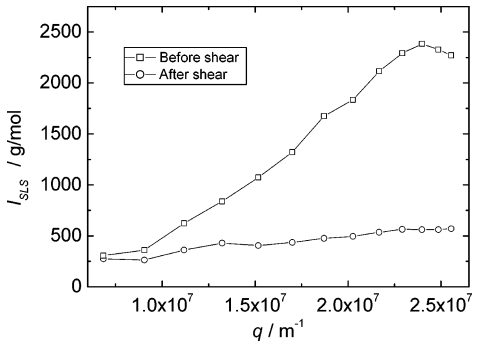

Figure 9. SLS data measured for sample B (□) before and (○) after capillary flow for 20 min.

The parameter $L_p = 510$ Å is approximately 2 orders of magnitude smaller than L_c values mentioned in the paragraph above. In addition, $L_p = 510$ Å does not satisfy the inequality a (= 57 Å) $\ll \lambda$ (= 663 nm) $< L_p$ necessary to apply the Kroy and Frey theory for semiflexible polymers.[27] Although this result might seem disappointing, it shows that the diffusion coefficients in Figure 7a are not related to an individual fiber. Indeed, to extract L_p from $g^{(1)}(q,t)$, the intensity correlation function should be measured with techniques that use shorter-wavelength radiation such as X-ray photon correlation spectroscopy.

The SLS data measured for sample B before and after shearing sample B for 20 min is shown in Figure 9. I_{SLS} before shear presents a broad structure factor peak, indicating a structure arising from fibril interaction. This peak is not present in I_{SLS} after shear, pointing to a weakening of the fibril interactions, probably due to fibril degradation.

The set of SAXS and light scattering results presented in this work are reasonable in the frame of previous findings. The Couette flow behavior of sample A was already reported in the literature.[18] Fibril degradation under shear flow was verified for $\dot{\gamma} > 100$ s^{-1}. In particular, fluorescence spectroscopy experiments revealed that for a shear rate of $\dot{\gamma} = 300$ s^{-1} fibril degradation started after the first 15 min under shear. It was speculated also that prior to the fibril degradation an increased fluorescence emission intensity under shear corresponded to initial orientation and partial deformation of the fibrils in the flow field.[18]

Conclusions

In this work we have described the capillary flow behavior of β-lg fibril gels containing fibril droplets and the shear flow alignment of β-lg fibers in dilute aqueous solutions.

POM and LSCM proved to be complementary techniques useful to study the fibril droplet flow behavior in β-lg fibril gels. In particular, LSCM directly provided images of the fibril matrix of the gel, without freezing or diluting the sample, as would be necessary for TEM or AFM studies. Our results showed that the capillary shear flow does not affect the fibril droplet size, and in this respect it is possible to state that they behave as compact colloidal particles under shear flow although not having a cross-linked fibril structure.

SAXS on dilute aqueous solutions indicates that the fibers can be aligned under capillary shear flow for the first 18 min after the shear has started, but this alignment is lost even after continuing to shear the sample for an additional $t = 42$ min. TEM experiments point to a reduction in the fibril network mesh size under shear, suggesting shear-flow-induced fibril breakup, the lost of orientation in the SAXS experiments probably being due to this phenomenon.

The dynamics of the β-lg fibers in dilute aqueous solutions before and after shear were examined by DLS. DLS indicated that β-lg fibers behave as semiflexible polymers before shear, but this behavior is lost after shearing the sample, probably due to shear-induced fibril degradation. Simultaneously, qualitative results were evaluated from SLS, which denoted a strong decrease of scattering intensity under shear, associated with a weakening of the fibril interactions under shear.

In a previous report[18] where β-lg fibers in solutions similar to our study were degraded under Couette flow, it was speculated that the shear flow degradation of β-lg fibers in the blood stream is a mechanism for amyloid disease propagation. Our results support this hypothesis, since we have verified β-lg fiber degradation using capillary shear flow, which more closely resembles flow in blood vessels.

Acknowledgment. V.C. and I.W.H. thank Anthony Gleeson for his assistance during SAXS experiments at the SRS. V.C. acknowledges Mr. S. K. Poutney for his support during the LSCM experiments, Dr. P. Harris for the training given on TEM, and Dr. T. Waigh for stimulating discussions.

References and Notes

(1) Ellis, R. J.; Pinheiro, T. J. T. *Nature (London)* **2002**, *416*, 483.
(2) Sipe, J. D. *Annu. Rev. Biochem.* **1992**, *61*, 947−975.
(3) Weisel, J.; Philips, G. J.; Choen, C. In *Molecular Biology of Fibrinogen and Fibrin*; Mosesson, M. W., Doolittle, R. F., Eds.; Annals of the New York Academy of Sciences 408; New York Academy of Sciences: New York, 1983.
(4) Kavanagh, G. M.; Clark, A. H.; Ross-Murphy, S. B. *Int. J. Biol. Macromol.* **2000**, *28*, 41.
(5) Kavanagh, G. M.; Clark, A. H.; Ross-Murphy, S. B. *Langmuir* **2000**, *16*, 9584.
(6) LeBon, C.; Nicolai, T.; Durand, D. *Macromolecules* **1999**, *32*, 6120.
(7) Lefevre, T.; Subirade, M. *Biopolymers* **2000**, *54*, 578.
(8) Aymard, P.; Nicolai, T.; Durand, D. *Macromolecules* **1999**, *32*, 2542−2552.
(9) Veerman, C.; Ruis, H.; Sagis, L. M. C.; van der Linden, E. *Biomacromolecules* **2002**, *3*, 869.
(10) Schokker, E. P.; Singh, H.; Pinder, D. N.; Creamer, L. K. *Int. Dairy J.* **2000**, *10*, 233.
(11) Nemoto, N.; Koike, A.; Osaki, K.; Koseki, T.; Doi, E. *Biopolymers* **1993**, *33*, 551.
(12) Renard, D.; Lefebvre, J. *Int. J. Biol. Macromol.* **1992**, *14*, 287.
(13) Gimel, J. C.; Durans, D.; Nicolai, T. *Macromolecules* **1994**, *27*, 583.
(14) Ikeda, S.; Morris, V. J. *Macromolecules* **2002**, *3*, 382.
(15) Arnaudov, L. N.; de Vries, R.; Ippel, H.; Van Mierlo, C. P. M. *Biomacromolecules* **2003**, *4*, 1614−1622.
(16) Wong, D. W. S.; Camirand, W. M.; Pavalath, A. E. *Crit. Rev. Food Sci. Nutr.* **1996**, *36*, 807.
(17) Gosal, W. S.; Clark, A. H.; Ross-Murphy, S. B. *Biomacromolecules* **2004**, *5*, 2408−2419.
(18) Hill, E. K.; Krebs, B.; Goodall, D. G.; Howlett, G. J.; Dunstan, D. E. *Biomacromolecules* **2006**, *7*, 10−13.
(19) Bernal, J. D.; Fankuchen, I. *J. Gen. Physiol.* **1941**, *25*, 111−146.
(20) Castelletto, V.; Hamley, I. W. *Polym. Adv. Technol.* **2006**, *17*, 137−144.
(21) Glatter, O.; Kratky, O., *Small Angle X-ray Scattering*; Academic Press: London, 1982.
(22) Berne, B. J.; Pecora, R. *Dynamic Light Scattering*; Wiley-Interscience: New York, 1976.
(23) Sagis, L. M. C.; Veerman, C.; van der Linden, E. *Langmuir* **2004**, *20*, 924−927.
(24) Krebs, M. R. H.; MacPhee, C. E.; Miller, A. F.; Dunlop, I. E.; Dobson, C. M.; Donald, A. M. *Proc. Natl. Acad. Sci. U.S.A.* **2004**, *101*, 14420−14424.
(25) Rogers, S. S.; Venema, P.; Sagis, L. M. C.; van der Linden, E.; Donald, A. M. *Macromolecules* **2005**, *38*, 2948−2958.

(26) Verheul, M.; Pedersen, J. A.; Roefs, S. P. F. M.; de Kruif, K. G. *Biopolymers* **1999**, *49*, 11−20.
(27) Kroy, K.; Frey, E. *Phys. Rev. E* **1997**, *55*, 3092−3101.
(28) Farge, E.; Maggs, A. C. *Macromolecules* **1993**, *26*, 5041−5044.
(29) Hardy, R. C.; Cottington, R. L. *J. Res. Natl. Bur. Stand.* **1949**, *42*, 573.

BM0605917